A New Process for Fuel Ethanol Dehydration Based on Modeling the Phase Equilibria of the Anhydrous $MgCl_2$ + Ethanol + Water System

Lanmu Zeng and Zhibao Li

Key Laboratory of Green Process and Engineering, Institute of Process Engineering, Chinese Academy of Sciences, Beijing 100190, China

DOI 10.1002/aic.14685

Published online November 24, 2014 in Wiley Online Library (wileyonlinelibrary.com)

The use of ethanol as a fuel for motor engines has attracted significant attention because of its possible environmental and economic advantages over fossil fuel. However, the energy demand for the ethanol dehydration process significantly impacts its production cost. A new and energy efficient process is developed on the basis of salt extractive distillation, which uses recycled $MgCl_2$ granules as a separating agent. Vapor-liquor-equilibria (VLE) data for the ternary $MgCl_2$ + ethanol + water system, and the three constituent binary systems were measured at 30, 60, 90, and 101.3 kPa. A large enhancement of relative volatility of the ethanol + water system in the presence of $MgCl_2$ is observed throughout the entire ethanol concentration range, which completely broke the azeotrope. The salt effect of $MgCl_2$ is thought to be the result of energetic interactions and the hydration equilibrium reaction of the Mg^{2+} ion with water molecules. The calculation results by the mixed-solvent electrolyte model embedded in the OLI platform equipped with new model interaction parameters and equilibrium constant (obtained via the regression of experimental VLE data), provided for a satisfactory means of simulating the $MgCl_2$ salt extractive distillation process. Finally, the process was proven feasible at the laboratory-scale resulting in large granules of recovered $MgCl_2$ and a product of 99.5 wt % ethanol. © 2014 American Institute of Chemical Engineers *AIChE J*, 61: 664–676, 2015

Keywords: fuel ethanol, anhydrous magnesium chloride, salt extractive distillation, vapor-liquor-equilibrium, thermodynamic modeling

Introduction

Reducing dependence on exhaustible fossil oil is important not only because of the environmental impact of burning fossil fuels, but also due to the political instability in oil-exporting countries. One of the most promising alternatives is fuel ethanol because little change is needed for the consumers, and ethanol can power a motor engine directly or with only minor modifications.[1] The main producers of fuel ethanol are the United States and Brazil where it is currently produced mainly from corn[2] and from sugarcane,[3] respectively. The annual production capacity of fuel ethanol is more than 13 billion gallons in the United States since 2010, which represents about 10% of the nation's motor fuel supply.[4] The potential feedstock for fuel ethanol is cellulosic materials such as corn stalks, wood chips, and switchgrass so that the pressure on food sources can be reduced.[5,6]

By fermentation of the sugar mixture, a broth containing 5–15 wt % ethanol is achieved.[7] The ethanol is then separated from the solid residue and concentrated to near the azeotropic point using conventional distillation. Further dehydration is needed to purify the ethanol to the fuel grade, whose water concentration should be below 1 vol % (about 98.4 wt %) as specified by the United States[8] or 0.3 wt % by the European Union.[9] The purification of ethanol to its anhydrous form is difficult and energy intensive due to the formation of the azeotrope of the ethanol + water system at about 96 wt % ethanol at atmospheric pressure. Furthermore, the relative volatility of ethanol to water approaches 1 at high ethanol concentrations.[7,10] To improve the energy efficiency of the fuel ethanol production process, it is critical to reduce the energy cost for ethanol dehydration.

Special techniques, such as azeotropic distillation,[11] extractive distillation,[12–14] membrane vapor permeation,[15] and molecular sieve adsorption,[16] are available for separating ethanol from water above the azeotropic composition. It is necessary for extractive distillation to add a miscible and high-boiling point entrainer such as ethylene glycol that can change the relative volatility of the mixture as well as break the azeotrope. A number of studies have been devoted to optimizing the distillation process to exhibit lower energy consumption.[17,18] Currently, molecular sieve adsorption is the state of art technique used in the U.S. fuel ethanol industry. Water molecules can be adsorbed by the molecular sieve, while the ethanol molecules are too large to enter into the inner structure of the molecular sieve. Thus, it is possible to dehydrate the ethanol-water mixture from near azeotropic concentrations.

Correspondence concerning this article should be addressed to Z. Li at zhibaoli@mail.ipe.ac.cn

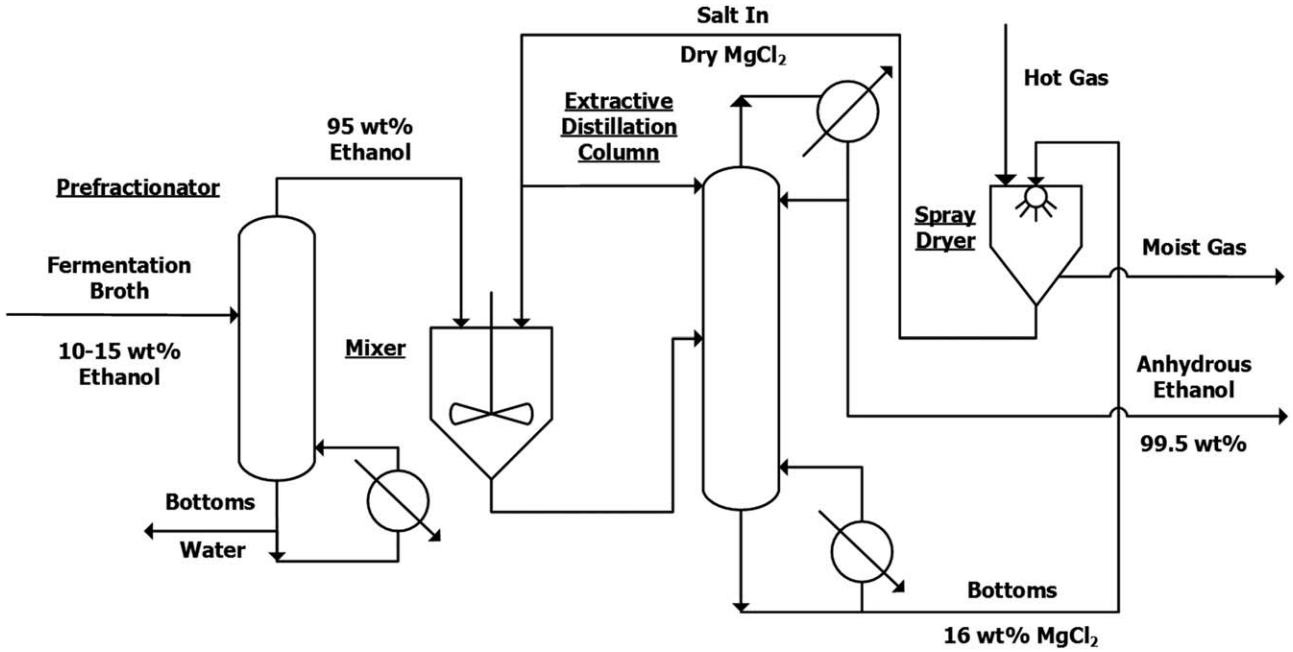

Figure 1. Illustrative flowsheet of the proposed process for fuel ethanol dehydration.

It is reported that the relative volatility of ethanol and the energy efficiency for ethanol dehydration can be greatly enhanced when a salt is dissolved in the ethanol + water system.[19–21] Less energy is required because the salt would not be vaporized through the distillation column, as compared to a liquid separating agent. Moreover, the requirement of latent heat decreases due to the higher relative volatility (less water is vaporized) with salt than the system without salt. For example, Hussain et al.[22] proposed a salt extractive distillation process for fuel ethanol production using $CaCl_2$ as a separating agent. Process simulation indicates a thermal energy saving of about 30% when compared with the molecular sieve adsorption process. Despite the benefits obtained by salt extractive distillation, recycling of the salts remains a crucial challenge. For example, the formation of dust during the regeneration of anhydrous $CaCl_2$ by sprayer drying can cause serious damage to handling equipment.[23]

The dehydration of magnesium chloride hexahydrate has been intensively studied by metallurgists for the application in the production of anhydrous $MgCl_2$.[24,25] Industrial practice has demonstrated that magnesium chloride hydrate granules with good flow properties can easily be obtained by heating bischofite at about 463 K. The Mg^{2+} ion in a solution containing ethanol and water has a strong tendency to form the hexaaquo complex with water ($Mg[H_2O]_6^{2+}$), generating a higher relative volatility. Furthermore, the large solubility of $MgCl_2$, similar to that of $CaCl_2$ in the ethanol + water system, would result in a wider window of concentrations through which the distillation process can operate. Therefore, $MgCl_2$ should act as a good separating agent in breaking the azeotrope of the ethanol + water system. Based on the properties of $MgCl_2$ and its hydrates, a new process for anhydrous ethanol production is proposed in this work, as shown in Figure 1. The fermentation broth is fed to the prefractionator in which the ethanol + water mixture is partially separated and a distillate with the ethanol concentration close to the azeotrope is obtained. The salt extractive distillation column receives the $MgCl_2$ + ethanol + water solution from the mixer as the feed and $MgCl_2$ is introduced at the top of the extractive column. Due to the salting-out effect of $MgCl_2$, the anhydrous ethanol is produced at the top of the column. The $MgCl_2$ is recovered by spray drying of the $MgCl_2$ aqueous solution collected from the bottom product of the extractive column.

The vapor-liquid-equilibria (VLE) of the $MgCl_2$ + ethanol + water system play a key role in developing and operating the new process. The VLE of various salts + ethanol + water systems have been published in the literatures. For example, Rieder and Thompson[26] and Vercher et al.[27] studied the effect of KNO_3 on the VLE behavior of the ethanol + water system. Vercher et al. measured the VLE data of the KAc + ethanol + water and KAc + NaAc + ethanol + water systems.[28] Meyer et al.[29] investigated the VLE of ethanol + water solutions containing $CaCl_2$ and NaCl at low-pressure. However, the VLE of the $MgCl_2$ + ethanol + water system have not been reported as far as we know. Yet work on the phase equilibria of aqueous $MgCl_2$ solutions mixed with other alcohols can be found, such as the $MgCl_2$ + 2-propanol + water system determined by Balaban et al.[30]

Properly representing the prominent solution chemistries and energetic interactions among the species are essential to thermodynamic modeling of the phase equilibria of an electrolyte system.[31] Some ions such as Mg^{2+} show a tendency to form hydrated ions where the water molecules are considered as a part of the ions.[32] As developed by Robinson and Stokes, the hydration number was introduced to build a relation between the apparent mean activity coefficient and the corresponding true activity coefficient in a hydrated solution.[33,34] However, the hydration number is found to be dependent on temperature and solution concentration,[35] thus it has limited applications in wide ranges of concentration and temperature. The hydration can also be determined by the chemical reaction between ions and water molecules (hydration equilibria) with the electrolyte model to describe the physical interactions, as presented by Lu and Maurer.[36,37]

In this work, the VLE data of the ternary $MgCl_2$ + ethanol + water system as well as the three constituent binary systems were determined experimentally. By including the hydration equilibrium reaction of Mg^{2+} with waters, the experimental data were represented by the mixed-solvent electrolyte (MSE) model embedded in the OLI software. Based on the model developed for the phase equilibria of the $MgCl_2$ + ethanol + water system, we performed laboratory-scale experiments to verify the feasibility of the proposed process. These included testing of the salt extractive distillation process, determination of the solubility of $MgCl_2$ in ethanol, and the recovery of the salt.

Experimental

Materials

The anhydrous magnesium chloride (99%, Alfa Aesar) was analytical grade without further purification. Analytical grade ethanol was provided by Beijing Chemical Plant with a minimum purity of 99.7%. De-ionized water with specific conductivity ($<0.1\ \mu S \cdot cm^{-1}$) was used.

Determination of the VLE

The VLE of the $MgCl_2$ + ethanol + water system were measured with a dual circulation still manufactured by Zhehua Instruments.[38,39] Figure 2 displays a schematic diagram of the dual circulation still. The vapor and liquid phases are both circulated in the still. The special design of the equilibrium chamber prevents boiling solution from mixing with the vapor phase. A magnetic stirrer provides a mixing effect and additional mechanical driving force for the circulation of the solution. The boiling is achieved by a heating pod and the heating power can be adjusted by a rheostat. The temperature for the condensation of the vapor phase was 275 K. To ensure no condensation occurs in the equilibrium chamber, the right side of the still is covered by a vacuum jacket. The pressure of the whole system was controlled as in Li et al.[40–42] An inclined ebulliometer[43] is connected with the still to indicate the pressure. The temperature of the still and ebulliometer is measured by calibrated mercury thermometers with an uncertainty of ± 0.15 K, which causes a pressure uncertainty of ± 0.6 kPa.

During each run, the dual circulation still was initially filled with a volume of about 100 mL of gravimetrically prepared solution using an electronic analytical balance (AL104, Mettler-Toledo) with an uncertainty of 0.0001 g while deionized water was added to the so called "reference ebulliometer." The whole system was subjected to low pressure and the liquid was heated to its boiling with rigorous stirring. Then the system was carefully adjusted to the desired pressure by monitoring the temperature of the reference ebulliometer because the pressure could be calculated from the boiling temperature of water. The temperatures of the ebulliometer corresponding to system pressures of 30, 60, 90, 101.3 kPa were 342.4, 359.2, 369.9, and 372.5 K, respectively. To establish the equilibrium, heating and circulation of the solutions were continued for 30 min after the temperatures of the still and ebulliometer were constant. When equilibrium was reached, the boiling temperature of the $MgCl_2$ + ethanol + water mixture was recorded. The liquid and vapor samples were collected with 2 mL plastic syringes. The experiment was then continued at higher pressure by introducing air into the system.

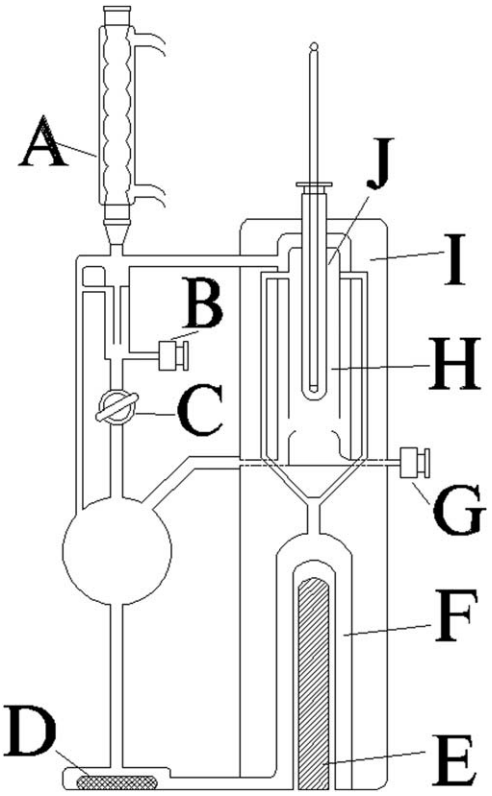

Figure 2. Schematic drawing of the dual circulation still.

A, condenser; B, vapor sampling port; C, valve; D, magnetic stirrer; E, heating rod; F, boiling chamber; G, liquid sampling port; H, equilibrium chamber; I, vacuum jacket; J, thermometer well.

Solubility determination

The dynamic method similar to that used by Gao and Li[44] was adopted. A known mass of ethanol solution was added to a 250-mL jacketed glass vessel equipped with magnetic stirrer. The temperature of the vessel was maintained within ± 0.1 K by circulating water from a thermostated bath. Known amounts of $MgCl_2$ were carefully added into the solution until a small amount of solid remained undissolved. The solubility could then be calculated from the mass of the added liquid ethanol and solid $MgCl_2$.

Preliminary distillation test

The extractive distillation was conducted using a jacketed glass column packed with glass helix rings ($\Phi 10 \times 4$ mm). The height and internal diameter of the column were 1 m and 50 mm (eight theoretical stages), respectively. Initially, 500 mL of the $MgCl_2$ + ethanol + water mixture was added to the reboiler and heated by an electrical heating unit (Maximum 0.5 kW thermal power). Ethanol and water vapor bubbled through the column to a water-cooled condenser. The column was first run at total reflux for about 1 h to approach steady state. When the steady state was reached, a total volume of 500 mL of prepared $MgCl_2$ + ethanol solution was introduced into the top of the column by a peristaltic pump. Condensed vapor samples together with the samples from stages 2 and 6 were taken periodically to determine their water concentration until the addition of salt was completed.

Decomposition of the residue

A quartz-fluidized bed was used for thermal decomposition of the residue collected from the reboiler after the distillation experiment. The temperature was controlled by an electrical heating mantle within ± 1 K. The experiment was initiated by adding the residue to the fluidized bed. N_2 gas at a flow rate of 0.11 L/min was injected into the bottom of the fluidized bed. Then the fluidized bed was heated to the desired temperature for 1 h. The obtained particles were stored in a desiccator for XRD and SEM analysis.

Chemical analysis and characterization

The concentration of Mg was measured by the chelation titration method with ethylene diaminetetraacetic acid, using Eriochrome black T as the indicator and NH_3-NH_4Cl as buffer solution. The water concentration of the sample was analyzed by the Karl-Fisher method using a type ZSD-2 automatic titrator manufactured by Shanghai Anting Electronic Instruments. The uncertainties of the Mg and water measurements were 0.0001 and 0.0005 mole fraction, respectively. The solid samples were characterized by x-ray diffractometer (XRD, X'Pert PRO MPD, PANalytical) and scanning electron microscopy (SEM, JEOL-JSM-6700F). The XRD patterns were recorded using Cu/Kα radiation operating at 40 kV/40 mA with a scanning rate of 0.02°/s.

Thermodynamic Modeling Framework

Chemistry of the $MgCl_2$ + ethanol + water system

The binary ethanol + water system is complicated by the addition of salts.[19,20] The interactions between ethanol and water can be altered as the molecules interact with the dissolved salts. The degree of dissociation of the salts in turn becomes a function of the solvent composition. Moreover, the ions of salts tend to form complexes with water or ethanol, which affect the volatility of selected components. For instance, Balaban et al. and Smirnova modeled the phase equilibria of aqueous-organic electrolyte systems by taking into account the hydration (ion with water) and solvation (ion with organic solvent) of cations.[30,45] The equilibrium constants, and the hydration and solvation numbers were treated as empirical parameters in their model. Ohe et al.[46,47] proposed a solvation model based on the assumption that the effect of salt is caused by the solvation of the ions and the solvated solvent cannot contribute to the VLE. The VLE of multi-component systems in the Ohe model can be predicted from the solvation numbers determined from binary solvents + salt systems data. In the Lu and Maurer's model,[36] cations and anions were both considered as hydrated. The hydration number is expressed as a function of temperature by an empirical equation. The physical interaction is represented by combining the Debye-Hückel law with the UNIQUAC model.

The physical interaction forces between the various species in solution, such as van der Waal forces, electrostatic attraction, and repulsion and hydrogen bonding, were described by the MSE model. $MgCl_2$ was regarded as completely dissociated while the hydration of anions was disregarded. The solvation of Mg^{2+} ion by ethanol was assumed to be negligible compared with the hydration by water. Although the hydration numbers in the previously proposed models were often substantiated by empirical equations, the hydration of the Mg^{2+} ion was assumed to be a hydration reaction with the fixed number of 6. In the presented model, the thermodynamic equilibrium constant for the hydration reaction is a function of temperature only.

By assuming a single thermodynamic entity for the Mg^{2+} ion with six waters of hydration, Pinsky and Gruber successfully modeled the osmotic coefficient data for aqueous $MgCl_2$ solutions using the non-random two-liquid (NRTL) model.[48] Also, independent experimental evidence for the hydration of Mg^{2+} ion with six water molecules was reported by Hunt and Friedman,[49] and Enderby et al.[50] from proton NMR and neutron diffraction studies. Based on these findings, the $Mg[H_2O]_6^{2+}$ ion, referred to as the Mg-water complex in this work, was assumed to be present in the $MgCl_2$ + ethanol + water system, and the hydration equilibrium reaction is expressed as

$$Mg[H_2O]_6^{2+} = Mg^{2+} + 6H_2O \tag{1}$$

The relevant thermodynamic equilibrium constant for reaction (1) is given by

$$K\left(Mg[H_2O]_6^{2+}\right) = \frac{\left(x_{Mg^{2+}}\gamma_{Mg^{2+}}\right)\left(a_{H_2O}\right)^6}{\left(x_{Mg[H_2O]_6^{2+}}\gamma_{Mg[H_2O]_6^{2+}}\right)} \tag{2}$$

where $K(Mg[H_2O]_6^{2+})$ is the mole-based thermodynamic equilibrium constant for $Mg[H_2O]_6^{2+}$.

Vapor-liquid equilibrium

The VLE of a given species, like ethanol, can be treated by the following relation

$$\text{ethanol(vapor)} = \text{ethanol(aq)} \tag{3}$$

When the system achieves thermodynamic equilibrium, the chemical potential of the vapor and aqueous species should be equal

$$\mu_{Vi} = \mu_{Vi}^o + RT\ln f_{Vi} = \mu_{Aqi} = \mu_{Aqi}^o + RT\ln a_{Aqi} \tag{4}$$

where μ_{Vi} is the chemical potential for the species i in vapor phase. Similarly μ_{Aqi} is the chemical potential for the species i in liquid phase. μ_{Vi}^0 and μ_{Aqi}^0 are the standard state chemical potential. R is the gas constant (8.314 J mol^{-1} K^{-1}) and T is the temperature (K). The fugacity of species i in the vapor phase f_{Vi}, is expressed as

$$f_{Vi} = Py_i\varphi_{Vi} \tag{5}$$

where P is the system pressure (atm), and y_i is the mole fraction of species i in the vapor phase. φ_{Vi} is the vapor phase fugacity coefficient of species i, which is calculated from the Soave−Redlich−Kwong (SRK) equation of state.[51] The activity of species i in the liquid phase a_{Aqi}, is written as

$$a_{Aqi} = x_i\gamma_i \tag{6}$$

where x_i is the mole fraction of species i in the liquid phase. γ_i is the activity coefficient of species i estimated by the activity coefficient model.

By introducing the thermodynamic equilibrium constant, K, for the vapor-liquid-equilibrium, the relationship between y_i and x_i is given as

$$K = \exp\left[\frac{\mu_{Aqi}^o - \mu_{Vi}^o}{RT}\right] = \frac{a_{Aqi}}{f_{Vi}} = \frac{x_i\gamma_i}{Py_i\varphi_{Vi}} \tag{7}$$

Activity coefficient and thermodynamic equilibrium constant

The activity coefficients for relevant species and thermodynamic equilibrium constants are essential for modeling the vapor-liquid-equilibrium. The MSE model proposed by Wang et al.[52] is a comprehensive model for the calculation of thermodynamic properties such as speciation and phase equilibria. The model is suitable for the $MgCl_2$ + ethanol + water system as the solvent in the model can be a mixture of organics and water. The thermodynamic equilibrium constant in the MSE model is estimated from the standard-state chemical potentials of all species that participate in the reaction. For the species in the liquid phase, the standard-state chemical potential is evaluated by the HKF model developed by Tanger and Helgeson.[53] In the situation where no accurate thermodynamic data exists, the value of K is calculated from an empirical equation.

The activity coefficient is a scale of the nonideality (excess properties) of the system, and it is derived from the excess Gibbs free energy of the solution

$$\ln \gamma_i = \left[\frac{\partial(n_{\text{total}}\, G^{ex}/RT)}{\partial n_i}\right]_{T,P,n_j} \tag{8}$$

The excess Gibbs free energy in the MSE model is composed of three terms

$$\frac{G^{ex}}{RT} = \frac{G^{ex}_{\text{LR}}}{RT} + \frac{G^{ex}_{\text{MR}}}{RT} + \frac{G^{ex}_{\text{SR}}}{RT} \tag{9}$$

where G^{ex}_{LR} represents the contribution of long-range electrostatic interactions; G^{ex}_{SR} is the short-range contribution resulting from molecule/molecule, molecule/ion, and ion/ion interactions; and an additional middle-range term G^{ex}_{MR} accounts for ionic interactions that are not included in the long-range term.

The Pitzer-Debye-Hückel expression is used for the long-range electrostatic contribution because of its empirical effectiveness in modeling aqueous electrolyte solutions. To account for the short-range interactions that exist at the immediate neighborhood of any species, the local composition based UNIQUAC model is selected. The excess Gibbs energy in the UNIQUAC model is calculated as a sum of a combinatorial and a residual term

$$\frac{G^{ex}_{\text{UNIQUAC}}}{RT} = \frac{G^{ex}_{\text{combinatorial}}}{RT} + \frac{G^{ex}_{\text{residual}}}{RT} \tag{10}$$

with

$$\frac{G^{ex}_{\text{combinatorial}}}{RT} = \left(\sum_i n_i\right)\left[\sum_i x_i \ln \frac{\phi_i}{x_i} + \frac{Z}{2}\sum_i q_i x_i \ln \frac{\theta_i}{\phi_i}\right] \tag{11}$$

$$\frac{G^{ex}_{\text{residual}}}{RT} = -\left(\sum_i n_i\right)\left[\sum_i q_i x_i \ln\left(\sum_j \theta_j \tau_{ij}\right)\right] \tag{12}$$

$$\theta_i = \frac{q_i x_i}{\sum_j q_j x_j} \tag{13}$$

$$\phi_i = \frac{r_i x_i}{\sum_j r_j x_j} \tag{14}$$

$$\tau_{ij} = \exp\left(-\frac{a_{ij}}{RT}\right) \tag{15}$$

where q_i and r_i are the surface area and volume-size parameters. The coordination number, Z, which represents the number of closely interacting molecules around a central molecule, is a constant with a value of 10. a_{ij} is the binary interaction parameter between species i and j ($a_{ij} \neq a_{ji}$). The dependence of a_{ij} on the temperature is expressed as

$$a_{ij} = Q0IJ + Q1IJ \times T + Q2IJ \times T^2 \tag{16}$$

where $Q0IJ$, $Q1IJ$, and $Q2IJ$ are adjustable short-range interaction parameters for the activity coefficient calculations in the MSE model.

The middle-range term is represented by a symmetrical second virial coefficient-type expression

$$\frac{G^{ex}_{\text{MR}}}{RT} = -\left(\sum_i n_i\right)\sum_i \sum_j x_i x_j B_{ij}(I_x) \tag{17}$$

where I_x is the mole fraction-based ionic strength. $B_{ij}(I_x)$ is a symmetric ($B_{ij}=B_{ji}$, and $B_{ii}=B_{jj}=0$) binary interaction parameter between species i and j (ion or molecule). $B_{ij}(I_x)$ is ionic strength-dependent and expressed by the following empirical expression

$$B_{ij}(I_x) = b_{ij} + c_{ij}\exp\left(-\sqrt{I_x + 0.01}\right) \tag{18}$$

where b_{ij} and c_{ij} are functions of temperature

$$b_{ij} = \text{BMD0} + \text{BMD1} \times T + \text{BMD2}/T + \text{BMD3} \times T^2 + \text{BMD4} \times \ln T \tag{19}$$

$$c_{ij} = \text{CMD0} + \text{CMD1} \times T + \text{CMD2}/T + \text{CMD3} \times T^2 + \text{CMD4} \times \ln T \tag{20}$$

where BMD0, BMD1, CMD0, and CMD1 etc are the adjustable middle-range interaction parameters used in the activity coefficient calculations.

For an aqueous electrolyte solution, the interactions between ion−ion and ion−neutral molecules are accounted for the middle-range interaction parameters unless the solution is very concentrated. In mixed solvent systems, the middle-range and short-range contributions should both be considered to account for molecular interactions between the electrolyte and the solvent molecules.[54] The neutral−neutral interactions, i.e., the interaction between ethanol and water, are represented by the short-range parameters.

Table 1. Isobaric VLE Data (Liquid-Phase Mole Fraction X_1, Vapor-Phase Mole Fraction y_1 and Temperature T) of the Binary Ethanol (1) + Water (2) System

P = 30 kPa			P = 60 kPa		
x_1	y_1	T/ K	x_1	y_1	T/ K
0.0978	0.4265	331.19	0.0832	0.3991	347.43
0.2596	0.5568	327.05	0.2544	0.5616	342.51
0.3813	0.6119	325.79	0.3833	0.5963	341.10
0.4894	0.6499	325.16	0.4879	0.6505	340.32
0.5959	0.6970	324.61	0.5923	0.6820	339.71
0.6982	0.7515	324.10	0.6965	0.7513	339.11
0.7987	0.8197	323.83	0.7999	0.8142	338.98
0.9028	0.9046	323.73	0.9039	0.9055	338.83
P = 90 kPa			P = 101.3 kPa		
0.0715	0.3718	358.25	0.0715	0.3718	364.16
0.2416	0.5527	352.46	0.2449	0.5414	355.51
0.3846	0.6039	351.03	0.3809	0.6059	354.18
0.4901	0.6547	350.27	0.4872	0.6455	353.21
0.5887	0.6946	349.66	0.5904	0.6948	352.60
0.6978	0.7528	349.15	0.6946	0.7532	351.99
0.8023	0.8161	348.81	0.7973	0.8163	351.75
0.9028	0.9019	348.81	0.9021	0.9019	351.70

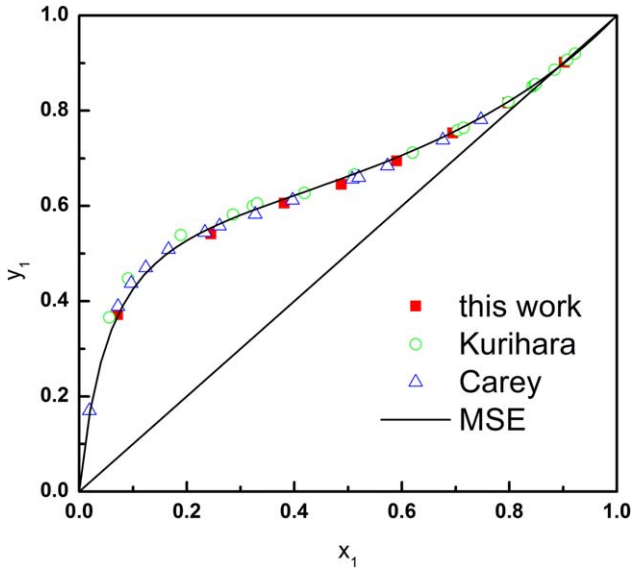

Figure 3. Equilibrium diagram of the binary ethanol (1) + water (2) system at 101.3 kPa.

[Color figure can be viewed in the online issue, which is available at wileyonlinelibrary.com.]

Results and Discussion

Verification of the apparatus

To verify the performance of the dual circulation still, the binary VLE data of the ethanol + water system at 30, 60, 90, and 101.3 kPa were measured and listed in Table 1. The VLE data measured at 101.3 kPa were compared with the data of Carey and Lewis[55] and Kurihara et al.[56] in Figure 3. The solid line represents the predictions by the MSE model. It can be seen that the present experimental and literature data are in good agreement, so the experimental apparatus and procedure were considered to be reliable to generate the VLE data. Also, the default MSE model parameters were shown to accurately describe the vapor-liquid equilibrium of the ethanol + water system.

VLE measurement of the binary $MgCl_2$ + ethanol and $MgCl_2$ + water systems

Table 2 lists the boiling points for the $MgCl_2$ + ethanol system up to about 0.06 (mole fraction) $MgCl_2$. The boiling points for the $MgCl_2$ + water system containing $MgCl_2$ in the mole fraction range of 8.92×10^{-3} to 8.995×10^{-2} are tabulated in Table 3. It was found that $MgCl_2$ was always soluble in these solutions and that no solids were precipitated during these experiments. The measured water concentration

Table 2. Isobaric Boiling Points of the Binary $MgCl_2$ (1) + Ethanol (2) System

	T/K			
x_1	30 kPa	60 kPa	90 kPa	101.3 kPa
0.00524	323.83	339.02	349.00	351.95
0.01002	323.98	339.17	349.11	352.10
0.01477	324.13	339.33	349.31	352.15
0.01994	324.23	339.48	349.41	352.35
0.02999	324.58	339.78	349.71	352.66
0.04003	324.99	340.19	350.17	353.17
0.04998	325.54	340.84	350.48	353.37
0.05979	326.00	341.50	351.14	354.18

Table 3. Isobaric Boiling Points of the Binary $MgCl_2$ (1) + Water (2) System

	T/ K			
x_1	30 kPa	60 kPa	90 kPa	101.3 kPa
0.00892	342.82	359.37	370.28	373.66
0.01763	343.43	360.08	370.95	373.96
0.02626	344.08	360.85	371.82	374.27
0.03477	344.95	362.54	372.74	375.73
0.04306	346.77	363.14	373.55	377.26
0.05125	347.74	364.57	375.18	378.68
0.06718	350.93	367.17	378.58	381.73
0.08289	355.10	372.63	383.25	386.40
0.08995	356.93	375.33	384.78	388.24

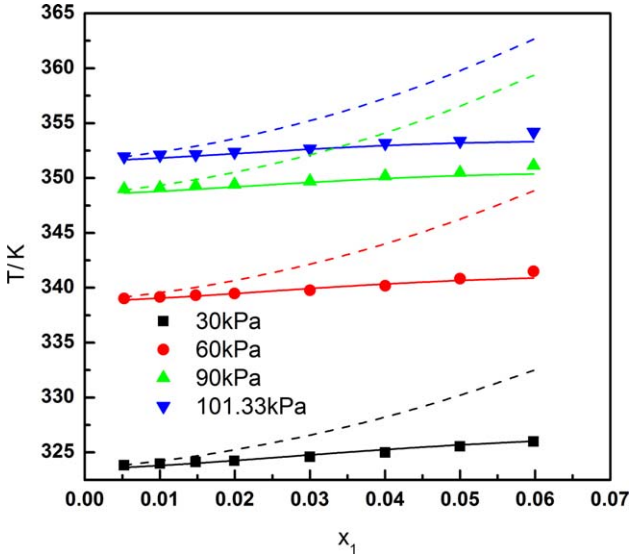

Figure 4. Boiling points of the binary $MgCl_2$ (1) + ethanol (2) system at 30, 60, 90, and 101.3 kPa.

[Color figure can be viewed in the online issue, which is available at wileyonlinelibrary.com.]

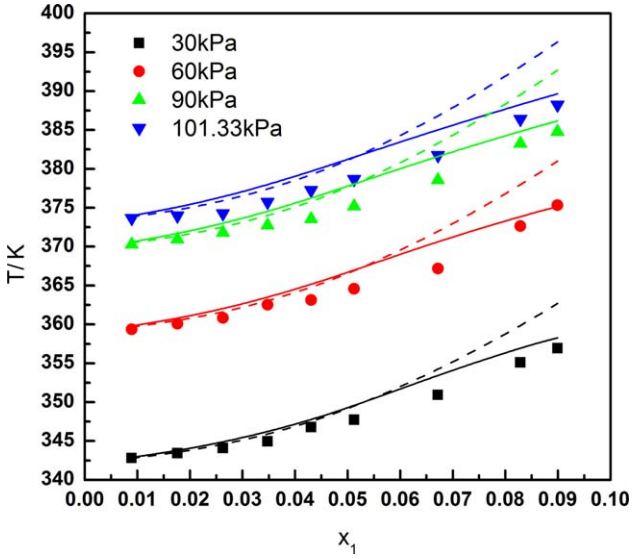

Figure 5. Boiling points of the binary $MgCl_2$ (1) + water (2) system at 30, 60, 90, and 101.3 kPa.

[Color figure can be viewed in the online issue, which is available at wileyonlinelibrary.com.]

Table 4. Isobaric VLE Data (Liquid-Phase Mole Fraction X_1, Vapor-Phase Mole Fraction y_1 and Temperature T) of the Ternary $MgCl_2$ (1) + Ethanol (2) + Water (3) System Containing 0.02 $MgCl_2$

x_1	x_2	x_2(Salt-Free)	y_2	*T*/ *K*
P = 30 kPa				
0.02123	0.0885	0.1294	0.4317	330.12
0.02110	0.1709	0.2097	0.4600	327.19
0.02101	0.2657	0.3023	0.6299	326.28
0.02128	0.3735	0.4082	0.6669	325.68
0.02075	0.4774	0.5090	0.7303	325.27
0.02163	0.5752	0.6059	0.7704	324.97
0.02118	0.6779	0.7057	0.7907	324.67
0.02099	0.7759	0.8013	0.8875	324.27
0.02130	0.8724	0.8960	0.9516	324.16
0.02167	0.9319	0.9546	0.9863	324.06
P = 60 kPa				
0.02116	0.0773	0.1183	0.4607	346.13
0.02137	0.1725	0.2117	0.5454	342.68
0.02122	0.2644	0.3013	0.6013	341.66
0.02152	0.3707	0.4058	0.6680	341.00
0.02061	0.4715	0.5030	0.7249	340.45
0.02048	0.5588	0.5882	0.7705	340.09
0.02158	0.6726	0.7011	0.8153	339.84
0.02134	0.7750	0.8009	0.8889	339.43
0.02241	0.8773	0.9020	0.9545	339.38
0.02230	0.9288	0.9523	0.9867	339.43
P = 90 kPa				
0.02177	0.0758	0.1179	0.4667	356.10
0.02187	0.1622	0.2026	0.5611	352.84
0.02173	0.2638	0.3016	0.6194	351.72
0.02164	0.3686	0.4039	0.6651	350.96
0.02087	0.4696	0.5015	0.7212	350.35
0.02187	0.5712	0.6023	0.7677	349.99
0.02228	0.6696	0.6990	0.8212	349.79
0.02174	0.7708	0.7973	0.8862	349.38
0.02264	0.8746	0.8997	0.9570	349.43
0.02322	0.9274	0.9518	0.9858	349.48
P = 101.3 kPa				
0.02204	0.0738	0.1166	0.4589	359.46
0.02194	0.1619	0.2024	0.5798	355.79
0.02173	0.2638	0.3016	0.6194	354.72
0.02183	0.3663	0.4020	0.6724	355.69
0.02109	0.4685	0.5008	0.7184	353.30
0.02223	0.5690	0.6007	0.7668	352.94
0.02241	0.6712	0.7007	0.8245	352.69
0.02197	0.7709	0.7976	0.8861	352.23
0.02285	0.8728	0.8982	0.9572	352.33
0.02350	0.9257	0.9504	0.9860	352.38

by the Karl-Fisher method after each test was below 0.005, indicating that the absorption of water was negligible. As illustrated in Figures 4 and 5, the boiling points for the $MgCl_2$ + ethanol and $MgCl_2$ + water systems increase with increasing $MgCl_2$ concentration due to the salting-out effect. However, the salting-out effect of $MgCl_2$ was weaker in the $MgCl_2$ + ethanol system than in the $MgCl_2$ + water system. For example, the increase of the boiling point after the addition of about 0.05 $MgCl_2$ is 1.82 K for the $MgCl_2$ + ethanol system, while the value is 5.53 K for the $MgCl_2$ + water system.

VLE measurement of the ternary $MgCl_2$ + ethanol + water system

In Tables 4–6, the VLE data for the ternary $MgCl_2$ (1) + ethanol (2) + water (3) system at pressure of 30, 60, 90 and 101.3 kPa are reported. The liquid-phase mole fraction of ethanol is also expressed on a salt-free basis in these tables. In all cases, $MgCl_2$ was completely dissolved at the boiling point of the solution. Figures 6 and 7 show the VLE of the ethanol + water system in the presence of 0.02 and 0.04 $MgCl_2$, respectively. It is observed that the addition of $MgCl_2$ to the ethanol + water system increases the ethanol concentration in the vapor phase. The salting-out effect of $MgCl_2$ monotonically increases with the increment of $MgCl_2$ concentration as displayed in Figure 8. The effect of pressure on the VLE was limited in the pressure range of 30−101.3 kPa as vapor composition retained almost the same value when the pressure was varied. By comparison with the salt-free VLE data in Figures 6 and 7, it is observed that the azeotropic point can be eliminated by the addition of only 0.02 $MgCl_2$.

The effectiveness of $MgCl_2$ in enhancing the relative volatility of ethanol to water at atmospheric pressure can be viewed in Figure 9. As can be seen in Figure 9, the relative volatility is enhanced throughout the entire ethanol concentration range in the presence of $MgCl_2$, indicating that $MgCl_2$ always preferentially attracts water. For example, the relative volatility in the ethanol + water mixture containing 0.95 ethanol is about 0.92, while it increases to 3.85 and

Table 5. Isobaric VLE Data (Liquid-Phase Mole Fraction X_1, Vapor-Phase Mole Fraction y_1 and Temperature T) of the Ternary $MgCl_2$ (1) + Ethanol (2) + Water (3) System Containing 0.04 $MgCl_2$

x_1	x_2	x_2(salt-free)	y_2	*T*/ *K*
30 kPa				
0.04086	0.0555	0.1339	0.5453	330.32
0.04346	0.1864	0.2638	0.6178	327.60
0.04236	0.2701	0.3421	0.7177	326.69
0.04187	0.3553	0.4228	0.7396	326.28
0.04306	0.4561	0.5211	0.7939	325.98
0.04331	0.5629	0.6235	0.7476	325.68
0.04301	0.6611	0.7170	0.8871	325.63
0.04332	0.7599	0.8118	0.9399	325.48
0.04280	0.8602	0.9072	0.9816	325.27
0.04401	0.9082	0.9544	0.9943	325.17
60 kPa				
0.04233	0.0742	0.1545	0.5426	346.23
0.04325	0.1622	0.2403	0.6389	343.08
0.04227	0.2630	0.3351	0.7090	342.07
0.04386	0.3662	0.4363	0.7358	341.61
0.04425	0.4570	0.5236	0.7870	341.26
0.04377	0.5672	0.6283	0.8273	341.05
0.04327	0.6563	0.7128	0.8824	340.85
0.04409	0.7567	0.8097	0.9388	340.80
0.04469	0.8546	0.9039	0.9810	340.65
0.04614	0.9080	0.9562	0.9937	340.65
90 kPa				
0.04258	0.0688	0.1498	0.5454	356.50
0.04417	0.1595	0.2394	0.6391	353.14
0.04311	0.2706	0.3438	0.7035	352.02
0.04466	0.3667	0.4380	0.7358	351.52
0.04433	0.4538	0.5207	0.7843	351.11
0.04368	0.5529	0.6145	0.8322	351.01
0.04410	0.6553	0.7128	0.8819	350.80
0.04463	0.7537	0.8074	0.9352	350.80
0.04595	0.8535	0.9041	0.9797	350.70
0.04687	0.9029	0.9522	0.9936	350.70
101.3 kPa				
0.04327	0.0709	0.1531	0.5546	359.77
0.04446	0.1462	0.2271	0.6366	356.10
0.04291	0.2535	0.3271	0.7062	354.98
0.04503	0.3507	0.4233	0.7312	354.57
0.04456	0.4536	0.5208	0.7815	354.06
0.04493	0.5543	0.6175	0.8291	353.96
0.04506	0.6564	0.7151	0.8814	353.86
0.04544	0.7539	0.8086	0.9370	353.81
0.04647	0.8507	0.9020	0.9776	353.75
0.04882	0.8975	0.9490	0.9933	353.75

Table 6. Isobaric VLE Data (Liquid-Phase Mole Fraction X_1, Vapor-Phase Mole Fraction y_1 and Temperature T) of the Ternary $MgCl_2$ (1) + Ethanol (2) + Water (3) System Containing 0.9 Ethanol

x_1	x_2	x_2(salt-free)	y_2	*T*/ *K*
30 kPa				
0.01138	0.8820	0.8947	0.9337	323.96
0.02130	0.8724	0.8960	0.9516	324.16
0.03294	0.8680	0.9043	0.9755	324.87
0.04280	0.8602	0.9072	0.9816	325.27
0.05484	0.8497	0.9098	0.9872	326.18
0.06519	0.8391	0.9105	0.9904	327.29
60 kPa				
0.01130	0.8807	0.8933	0.9308	339.13
0.02241	0.8773	0.9020	0.9545	339.38
0.03376	0.8672	0.9044	0.9727	340.09
0.04469	0.8546	0.9039	0.9810	340.65
0.05612	0.8451	0.9068	0.9862	341.66
0.06713	0.8331	0.9069	0.9889	342.88
90 kPa				
0.01160	0.8809	0.8938	0.9305	349.08
0.02264	0.8746	0.8997	0.9570	349.43
0.03462	0.8664	0.9045	0.9724	350.09
0.04595	0.8535	0.9041	0.9797	350.70
0.05772	0.8396	0.9033	0.9851	351.72
0.06792	0.8313	0.9060	0.9879	353.14
101.3 kPa				
0.01173	0.8809	0.8939	0.9293	352.02
0.02285	0.8728	0.8982	0.9572	352.33
0.03545	0.8615	0.9007	0.9720	353.14
0.04647	0.8507	0.9020	0.9776	353.75
0.05968	0.8360	0.9018	0.9842	354.87
0.06940	0.8274	0.9038	0.9873	356.40

8.90 when 0.02 and 0.04 $MgCl_2$ is added, respectively. It is interesting to note that the relative volatility increases with the increasing ethanol concentration above the 0.89 azeotrope of the ethanol + water system.

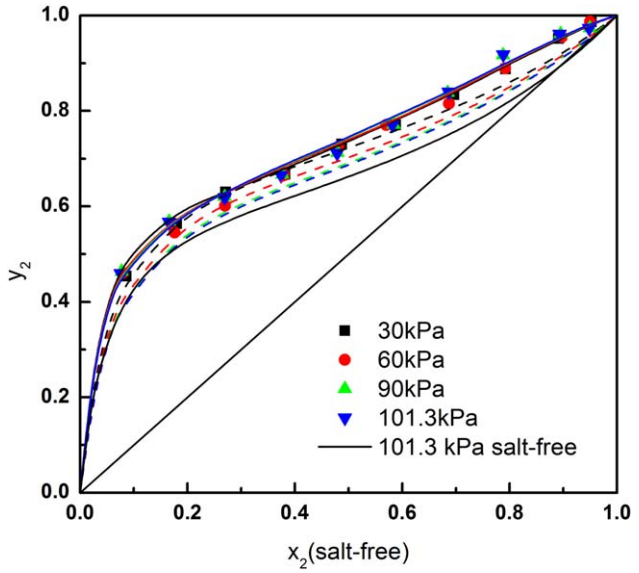

Figure 6. Isobaric VLE diagram of the ternary $MgCl_2$(1) + ethanol (2) + water (3) system containing 0.02 $MgCl_2$ at 30, 60, 90, and 101.3 kPa; the dashed lines represent the estimated vapor phase composition by the default databank; the solid lines represent the calculated values by the regressed parameters.

[Color figure can be viewed in the online issue, which is available at wileyonlinelibrary.com.]

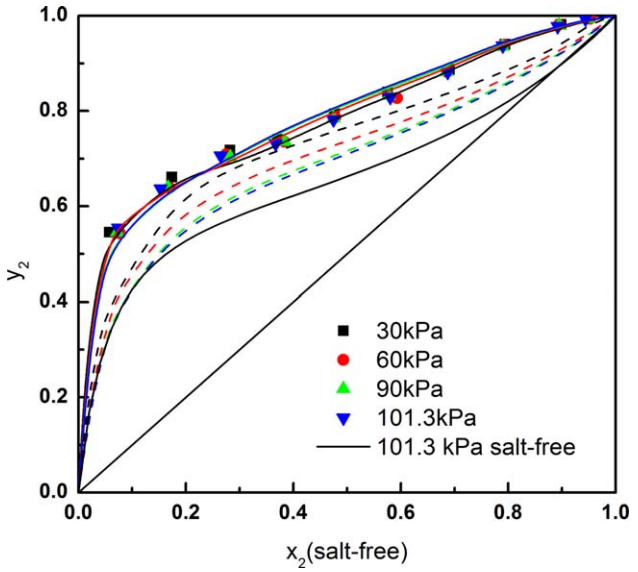

Figure 7. Isobaric VLE diagram of the ternary $MgCl_2$(1) + ethanol (2) + water (3) system containing 0.04 $MgCl_2$ at 30, 60, 90, and 101.3 kPa; the dashed lines represent the estimated vapor phase composition by the default databank; the solid lines represent the calculated values by the regressed parameters.

[Color figure can be viewed in the online issue, which is available at wileyonlinelibrary.com.]

Model parameterization

In order to test the capability of existing MSE model parameters (available in the software package Stream-

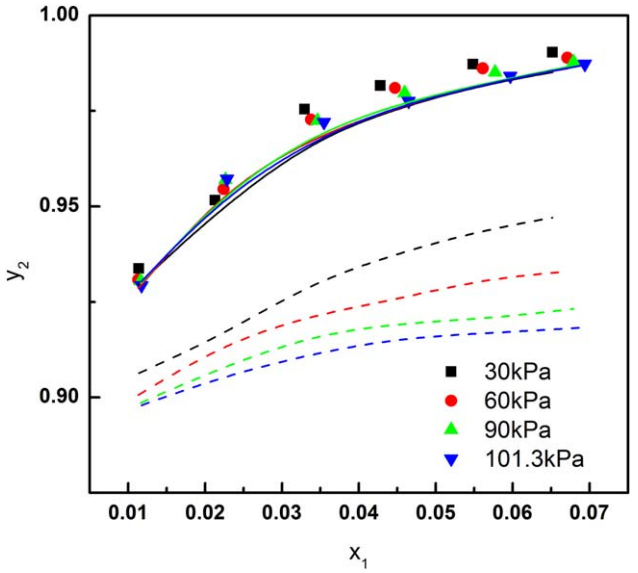

Figure 8. Isobaric VLE diagram of the ternary $MgCl_2$(1) + ethanol (2) + water (3) system containing 0.9 ethanol at 30, 60, 90, and 101.3 kPa; the dashed lines represent the estimated vapor phase composition by the default databank; the solid lines represent the calculated values by the regressed parameters.

[Color figure can be viewed in the online issue, which is available at wileyonlinelibrary.com.]

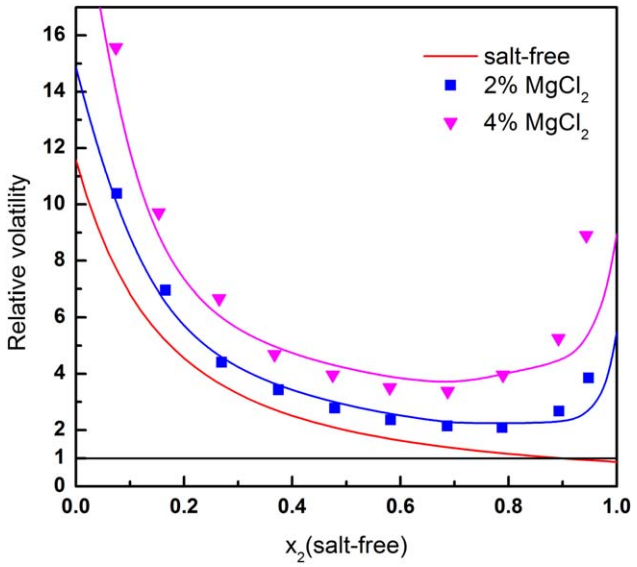

Figure 9. Relative volatility of ethanol to water as a function of ethanol concentration; the solid lines represent the predictions by the new model.

[Color figure can be viewed in the online issue, which is available at wileyonlinelibrary.com.]

Analyzer 9.0) for predicting the VLE data, the experimental data were calculated by the default parameters and the results are plotted in Figures 4–8 as dashed lines. Figures 4 and 5 show the predicted boiling points of the $MgCl_2$ + ethanol and $MgCl_2$ + water systems are larger than the experimental values, suggesting that the default parameters underestimate the salt effect of $MgCl_2$. And the deviations become larger when the concentration of $MgCl_2$ increases. As it can be observed in Figures 6–8, OLI's predictions of ethanol vapor composition are lower than the measured data especially in the ethanol rich zone. Moreover, the default parameters yield a dependence of pressure on the vapor composition.

To improve the model's performance, the middle-range interaction parameters for Mg^{2+}−ethanol, Cl^-—ethanol, $Mg^{2+}-Cl^-$, $Mg[H_2O]_6^{2+}-Mg^{2+}$, $Mg[H_2O]_6^{2+}-Cl^-$, and $Mg[H_2O]_6^{2+}$−ethanol, and the short-range interaction parameters for Mg^{2+}−ethanol and Cl^-—ethanol, together with the K value of the Mg-water complex, were regressed with the experimental data. The obtained parameters are listed in Tables 7 and 8. The K value of the Mg-water complex is

$$\log K = 7.400825 - \frac{2987.877}{T} \tag{21}$$

The short-range parameters for ethanol−water were directly used without any adjustment, as the default parameters were satisfactory; these are tabulated in Table 8. The surface area q_i and volume size r_i for various species are listed in Table 9. The q_i and r_i for ethanol and water are taken from the default databank while the values from the work of Mohs and Gmehling[57] are used for Mg^{2+} and Cl^- ions . For the Mg-water complex, the method presented by Lu and Maurer[36] is used to estimate the values of q_i and r_i.

The VLE data calculated by the new parameters are displayed as solid lines in Figures 4–8. As can be seen in Figure 4, the results predicted by new model parameters are in good agreement with the experimental boiling points of the binary $MgCl_2$ + ethanol system with a percent average absolute deviation (AAD) of 0.33 %. For the boiling point of the binary $MgCl_2$ + water system, Figure 5 shows that the new parameters closely reflect the experimental value with an AAD of 1.66 %, especially when the pressure is less than 60 kPa. Figures 6–8 illustrate that the calculated ethanol vapor composition by the new model in the ternary $MgCl_2$ + ethanol + water system is consistent with the experimental data, and the AAD is improved from 6.92 % by the default parameters to 1.36 %. It is worth to note in Figure 8 that the model's results at high ethanol concentration are not so good compared with the low-ethanol concentration region. The reason for the model performance at high ethanol concentration is the solution chemistry of $MgCl_2$ is different with the solution, in which little fraction of water molecules tends to solvate the Mg^{2+} and Cl^- ions. Figure 9 shows that the deviations between the model's predictions for the

Table 7. MSE Middle-Range Interaction Parameters[a]

Species	Mg^{2+}–Ethanol	Cl^-–Ethanol	Mg^{2+}–Cl^-	$Mg[H_2O]_6^{2+}$–Mg^{2+}	$Mg[H_2O]_6^{2+}$–Cl^-	$Mg[H_2O]_6^{2+}$–Ethanol
BMD0	−2.967503	−2.299666	−2.177395	−8.318294	−2.327875	−2.801383
BMD1	-1.0431908×10^{-2}	-7.7084982×10^{-3}	-2.3650963×10^{-4}	2.1075612×10^{-2}	-9.0246100×10^{-4}	2.8220766×10^{-3}
BMD2	−319.0962	−382.4392	−912.0105	−0.3843217	−1383.404	−2675.744
CMD0	0	0	−3.317551	0	0	0
CMD1	0	0	-1.9268539×10^{-3}	0	0	0
CMD2	0	0	−322.7178	0	0	0

[a]For all of the species pairs, BMD3, BMD4, CMD3, and CMD4 are set equal to zero.

Table 8. MSE Short-Range Interaction Parameters[a]

Species		Q0IJ	Q1IJ	Q2IJ
Ethanol	Water	118.7308	15.42545	-2.989896×10^{-2}
Water	Ethanol	−3170.838	10.56956	-5.334714×10^{-3}
Mg^{2+}	Ethanol	−3513.797	−26.85364	0
Ethanol	Mg^{2+}	−2912268	−1742201	0
Cl^-	Ethanol	−4861.032	-5.2721032×10^{-2}	0
Ethanol	Cl^-	−167373.2	2941.452	0

[a]Parameters for ethanol–water are retrieved from the MSEPUB databank in the OLI software.

Table 9. Surface Area q_i and Volume Size r_i for Various Species

Species	q_i	r_i	Refs
Ethanol	2.588	2.5755	a
Water	1.4	0.92	a
Mg^{2+}	0.1484	0.0571	b
Cl^-	0.9809	0.9699	b
$Mg[H_2O]_6^{2+}$	2.047	2.923	c

[a]MSEPUB databank in the OLI software.
[b]Mohs and Gmehling.[57]
[c]Estimated in this work.

relative volatility and the experimental values are relatively small when the ethanol concentration is less than 0.8. However, the model underestimates the relative volatility at ethanol concentration higher than 0.8. The relative volatility is very sensitive to the value of vapor composition at high ethanol concentration so that a small deviation of ethanol vapor composition could yield a significant error of the relative volatility. Moreover, the new middle-range interaction parameters (Mg^{2+}–Cl^-, $Mg[H_2O]_6^{2+}$–Mg^{2+}, $Mg[H_2O]_6^{2+}$–Cl^-) along with the K value for the Mg-water complex were verified by comparing the calculated value with literature data. Figure 10 displays the vapor pressure of the binary $MgCl_2$ + water system at various temperatures and $MgCl_2$ concentrations reported by Sako et al.[58] Figure 11 represents the osmotic coefficients of the aqueous $MgCl_2$ solutions determined at 298.15 K by Rard and Miller.[59] Both the vapor pressures and osmotic coefficients are successfully reproduced by the new parameters with an AAD of 2.22 and 4.34 %, respectively.

Application of the new model

The effect of $MgCl_2$ on the activity coefficients of ethanol and water was analyzed by the new model. Figure 12 shows that the activity coefficient of ethanol is enhanced by the addition of $MgCl_2$, suggesting that ethanol becomes more volatile. For example, the activity coefficient of ethanol increases from 3.08 to 3.55 and 4.12 when adding 0.02 and 0.04 $MgCl_2$ to the ethanol + water mixture containing 0.1 ethanol, respectively. The activity coefficient of water decreases in the presence of $MgCl_2$ especially in the ethanol rich region, which contributes to the increasing relative volatility of ethanol over water.

To investigate the effect of the hydration equilibrium reaction on the VLE of the ethanol + water system, the amount

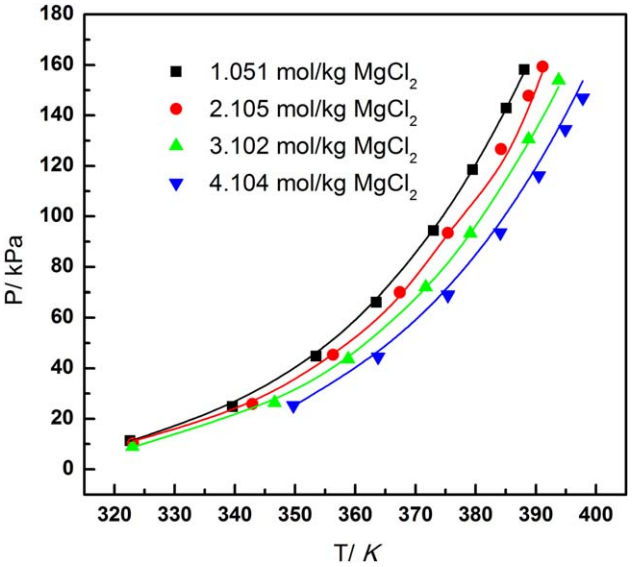

Figure 10. Vapor pressure of the binary $MgCl_2$ + water system as a function of temperature reported by Sako et al.; the solid lines represent the predictions by the model.

[Color figure can be viewed in the online issue, which is available at wileyonlinelibrary.com.]

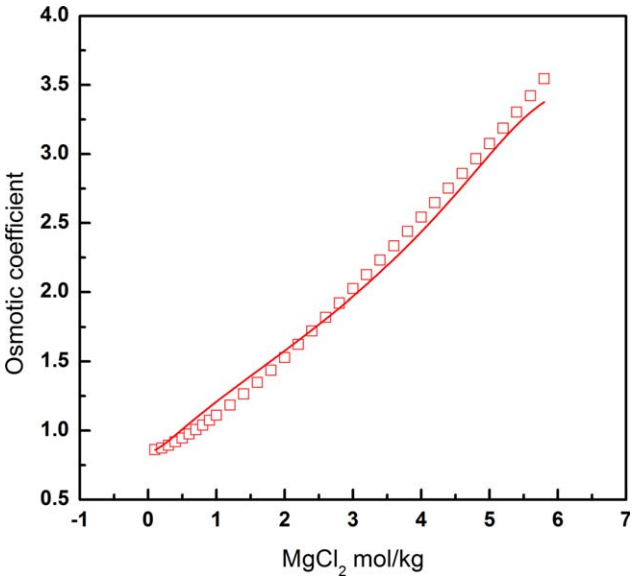

Figure 11. Osmotic coefficients of the binary $MgCl_2$ + water system measured at 298.5 K by Rard and Miller.; the solid lines represent the predictions by the new model.

[Color figure can be viewed in the online issue, which is available at wileyonlinelibrary.com.]

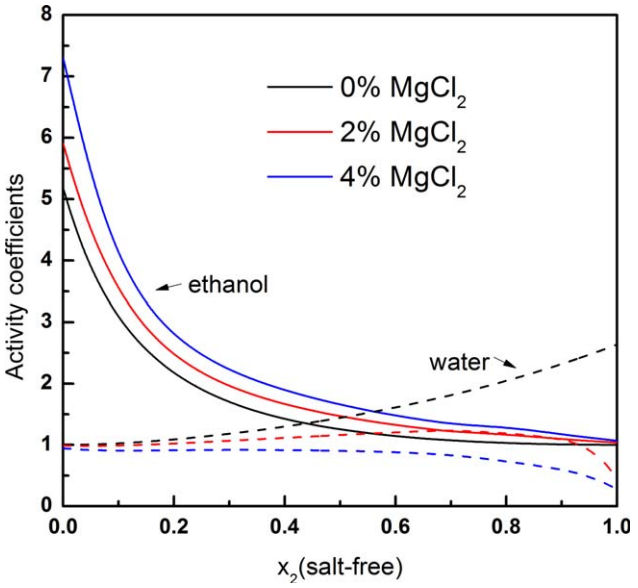

Figure 12. Activity coefficients of ethanol (solid lines) and water (dashed lines) in the boiled ternary $MgCl_2$(1) + ethanol (2) + water (3) system calculated by the new model.

[Color figure can be viewed in the online issue, which is available at wileyonlinelibrary.com.]

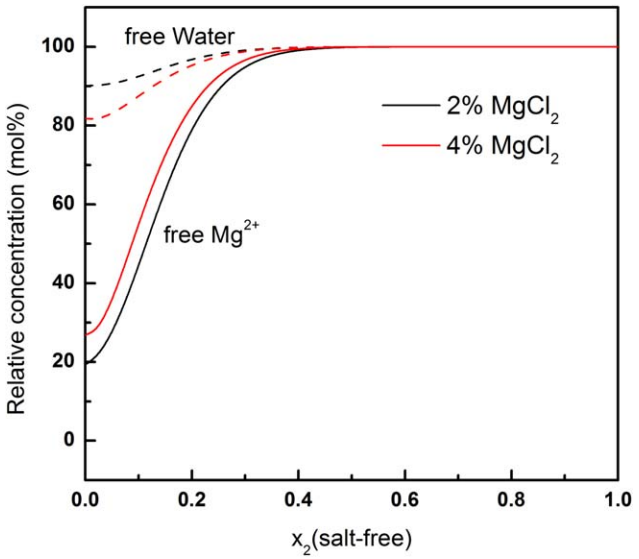

Figure 13. Relative concentration of free Mg^{2+} (solid lines) and water (dashed lines) in the boiled ternary $MgCl_2$(1) + ethanol (2) + water (3) system calculated by the new model.

[Color figure can be viewed in the online issue, which is available at wileyonlinelibrary.com.]

of "free" Mg^{2+} and water as a function of ethanol concentration were calculated by the new model. It can be observed in Figure 13 that the relative concentration of free Mg^{2+} and water increase with the increasing ethanol concentration. Therefore, the maximum value of the relative concentration of the Mg-water complex is achieved when the concentration of ethanol equals zero, which is 80% in the system containing 0.02 $MgCl_2$. The amount of Mg-water complex can be ignored when the ethanol concentration is higher than 0.4. In addition to the change of activity coefficients, the formation of the Mg-water complex in the water rich region which reduces the amount of free water, also contributes to the effect of $MgCl_2$ in altering the VLE behavior of the ethanol + water system.

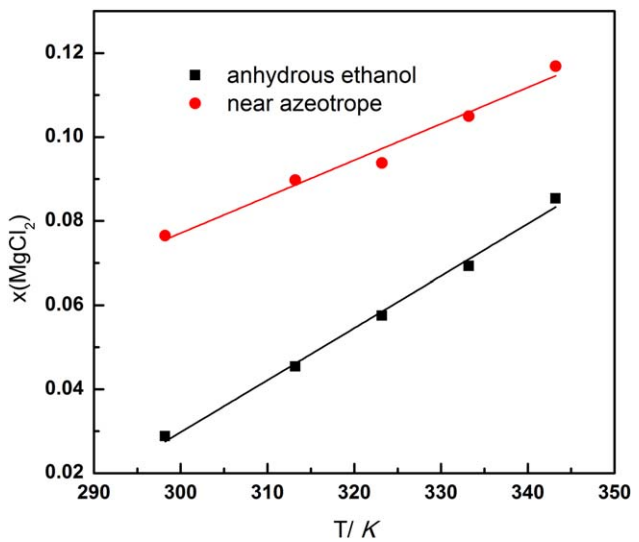

Figure 14. Experimental solubility of $MgCl_2$ in ethanol as a function of temperature.

[Color figure can be viewed in the online issue, which is available at wileyonlinelibrary.com.]

Table 10. Salt Extractive Distillation Operating Parameters

Parameters	Value
Theoretical stage number	8
Operating pressure	1 atm
Distillate flow rate	0.648 $L{\cdot}h^{-1}$
Reflux ratio	0.93
Reboiler $MgCl_2$ mole fraction	0.07
Reboiler ethanol mole fraction	0.66
Reboiler water mole fraction	0.27
Salt feed flow rate	0.366 $L{\cdot}h^{-1}$
Feed $MgCl_2$ mole fraction	0.02

Solubility of $MgCl_2$ in ethanol

Because $MgCl_2$ has to first dissolve in the feed solution, its solubility in ethanol needs to be known. Figure 14 shows the experimental solubility of $MgCl_2$ measured in this work in anhydrous ethanol and ethanol + water solution near the azeotropic point (0.84 ethanol) in the temperature range 298.2–343.2 K. It can be seen that the solubility increases gradually with increasing temperature. The solubility in the near azeotrope mixture is higher than that in anhydrous ethanol. For example, the equilibrium concentration of $MgCl_2$ in anhydrous ethanol is 0.0288 at room temperature. In contrast, it increases to 0.0765 in the near azeotrope mixture. The experimental solubility data also indicate that no solid would precipitate out during the VLE measurements as the concentration of $MgCl_2$ is below the solubility limit.

Laboratory-scale test

The new process for ethanol dehydration includes two key steps: salt extractive distillation and salt recovery. The semi-continuous laboratory-scale distillation was performed using the procedure mentioned before under the operating parameters listed in Table 10. The variation of water concentration as a function of time at different parts of the column (top, stages 2 and 6) is plotted in Figure 15. It can be seen that the water concentration of the product is about 4 wt % before $MgCl_2$ was introduced (−10min). As ethanol

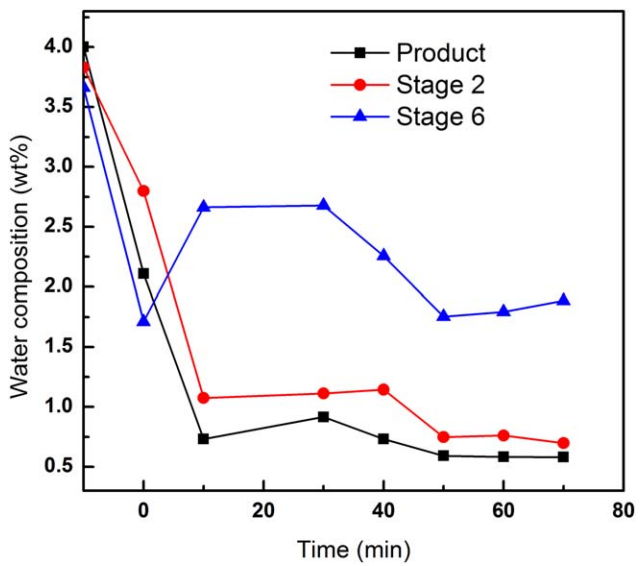

Figure 15. Variation of the water concentration in the stages and product.

[Color figure can be viewed in the online issue, which is available at wileyonlinelibrary.com.]

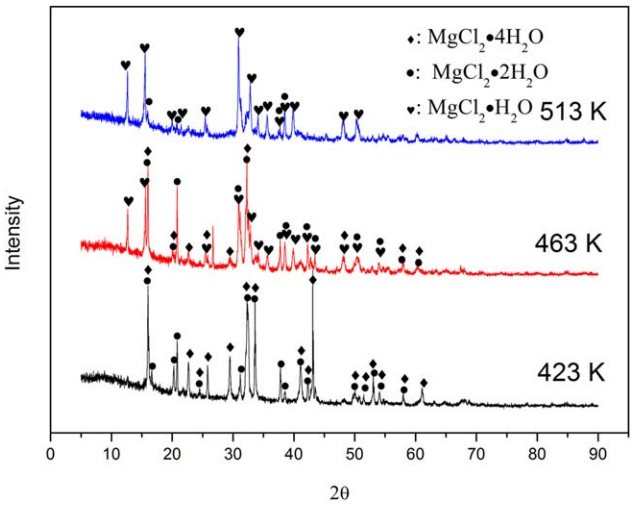

Figure 16. XRD patterns of the dried $MgCl_2 \cdot xH_2O$ prepared at different temperatures.

[Color figure can be viewed in the online issue, which is available at wileyonlinelibrary.com.]

becomes less volatile above the azeotropic point, the water concentration gradually increases from the bottom to the top of the column. With the introduction of $MgCl_2$, the water concentration of the product dramatically decreases to about 0.5 wt %, which satisfies the requirement of the ASTM standard.[8] Higher water concentrations were observed at the lower stage of the column due to the salting-out effect of $MgCl_2$.

The thermal decomposition of the residue was carried out at 423, 463, and 513 K. Figure 16 shows the XRD patterns of the obtained solids at different temperatures. It can be seen that the solid is a mixture of hydrated magnesium chlorides ($MgCl_2 \cdot xH_2O$) with different amounts of water. Peaks of $MgCl_2 \cdot 4H_2O$ and $MgCl_2 \cdot 2H_2O$ were detected when dried at 423 K, while the obtained solid was mainly composed of $MgCl_2 \cdot 2H_2O$ and $MgCl_2 \cdot H_2O$ at 463 K. Further increasing the temperature to 513 K results in $MgCl_2 \cdot H_2O$ as the major phase. However, the formation of HCl gas, which is harmful to motor engines, was observed during the decomposition experiment at 513 K. So the temperature of 463 K seems to be the most suitable for decomposition because it balances the dehydration with the prevention of HCl formation. Figure 17 displays an SEM image of the $MgCl_2 \cdot xH_2O$ prepared at 463 K. As can be seen in Figure 17, the small particles of $MgCl_2 \cdot xH_2O$ are strongly aggregated to form big granules.

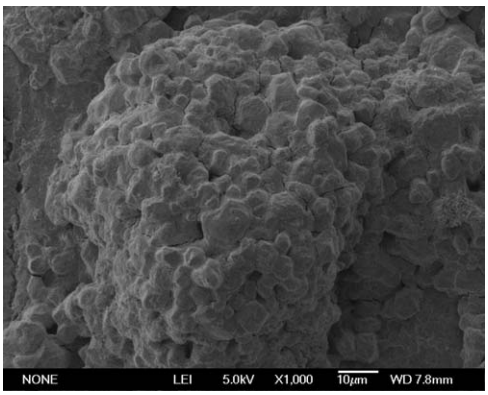

Figure 17. SEM image of the dried $MgCl_2 \cdot xH_2O$ prepared at 463 K.

Conclusions

A new process for fuel ethanol dehydration aiming to reduce the energy requirement based on the phase equilibria of the $MgCl_2$ + ethanol + water system was proposed and proven feasible at the laboratory-scale. The VLE of the ethanol + water mixtures are fundamentally changed by adding $MgCl_2$ as determined using the dual circulation still. The relative volatility of the ethanol + water system in the presence of $MgCl_2$ even increases with increasing ethanol concentration above the azeotropic point. A self-consistent model was constructed by considering the hydration of $MgCl_2$ as hydration equilibrium reaction for predicting the VLE of the ternary $MgCl_2$ + ethanol + water system, as well as the binary $MgCl_2$ + ethanol, $MgCl_2$ + water and ethanol + water systems. With the regressed middle-range interaction parameters for $Mg^{2+}-$ethanol, Cl^--ethanol, $Mg^{2+}-Cl^-$, $Mg[H_2O]_6^{2+}-Mg^{2+}$, $Mg[H_2O]_6^{2+}-Cl^-$, and $Mg[H_2O]_6^{2+}-$ ethanol, and the short-range interaction parameters for $Mg^{2+}-$ethanol and Cl^--ethanol, and the K value of the Mg-water complex, the correlated VLE data showed good agreement with experimental data. The experimental results and thermodynamic model developed in this work provide fundamental knowledge for the further development and simulation of the ethanol dehydration process using $MgCl_2$ as separating agent.

Acknowledgments

The authors are grateful to the financial support of National Natural Science Foundation of China (Grant No. 21476235 and 21206165), National Basic Research Program of China (973 Program with Grant No. 2013CB632605) and the Science and Technology Planning Project of Qinghai Province (2012-G-213A).

Literature Cited

1. Andersen VF, Anderson JE, Wallington TJ, Mueller SA, Nielsen OJ. Vapor pressures of alcohol−gasoline blends. *Energy Fuels*. 2010;24:3647–3654.
2. Karuppiah R, Peschel A, Grossmann IE, Martín M, Martinson W, Zullo L. Energy optimization for the design of corn-based ethanol plants. *AIChE J*. 2008;54:1499–1525.
3. Goldemberg J. Ethanol for a sustainable energy future. *Science* 2007;315:808–810.
4. Annual Industry Outlook. Available at: http://www.ethanolrfa.org/pages/annual-industry-outlook, Accessed on 7 April 2014.
5. Andersen FE, Díaz MS, Grossmann IE. Multiscale strategic planning model for the design of integrated ethanol and gasoline supply chain. *AIChE J*. 2013;59:4655–4672.
6. Martín M, Grossmann IE. Energy optimization of bioethanol production via hydrolysis of switchgrass. *AIChE J*. 2012;58:1538–1549.
7. Kwiatkowski JR, McAloon AJ, Taylor F, Johnston DB. Modeling the process and costs of fuel ethanol production by the corn dry-grind process. *Ind Crops Prod*. 2006;23:288–296.
8. D02 Committee. *Specification for Ethanol Fuel Blends for Flexible-Fuel Automotive Spark-Ignition Engines*. West Conshohocken, PA: ASTM International, 2013.
9. Energy: Biofuels - Standards - European Commission. Available at: http://ec.europa.eu/energy/renewables/biofuels/standards_en.htm, Accessed on 16 February 2014.
10. Lee FM, Pahl RH. Solvent screening study and conceptual extractive distillation process to produce anhydrous ethanol from fermentation broth. *Ind Eng Chem Proc Des Dev*. 1985;24:168–172.
11. Pienaar C, Schwarz CE, Knoetze JH, Burger AJ. Vapor–liquid–liquid equilibria measurements for the dehydration of ethanol,

isopropanol, and n-propanol via azeotropic distillation using dipe and isooctane as entrainers. *J Chem Eng Data*. 2013;58:537–550.
12. Dhanalakshmi J, Sai PST, Balakrishnan AR. Effect of inorganic salts on the isobaric vapor–liquid equilibrium of the ethyl acetate-ethanol system. *J Chem Eng Data*. 2013;58:560–569.
13. Kumar S, Prasad R. Effect of diaminomethanal on the vapor-liquid equilibria of the ethanol + water system at atmospheric pressure. *J Chem Eng Data*. 2010;55:2581–2585.
14. Pinto RTP, Wolf-Maciel MR, Lintomen L. Saline extractive distillation process for ethanol purification. *Comput Chem Eng*. 2000;24: 1689–1694.
15. Vane LM, Alvarez FR, Rosenblum L, Govindaswamy S. Efficient ethanol recovery from yeast fermentation broth with integrated distillation–membrane process. *Ind Eng Chem Res*. 2013;52:1033–1041.
16. Simo M, Sivashanmugam S, Brown CJ, Hlavacek V. Adsorption/ desorption of water and ethanol on 3A zeolite in near-adiabatic fixed bed. *Ind Eng Chem Res*. 2009;48:9247–9260.
17. Ramírez-Márquez C, Segovia-Hernández JG, Hernández S, Errico M, Rong BG. Dynamic behavior of alternative separation processes for ethanol dehydration by extractive distillation. *Ind Eng Chem Res*. 2013;52:17554–17561.
18. Vázquez-Ojeda M, Segovia-Hernández JG, Hernández S, Hernández-Aguirre A, Kiss AA. Design and optimization of an ethanol dehydration process using stochastic methods. *Sep Purif Technol*. 2013;105: 90–97.
19. Meranda D, Furter WF. Salt effects on vapor-liquid equilibrium: some anomalies. *AIChE J*. 1974;20:103–108.
20. Furter WF. Extractive distillation by salt effect. In: Dimitrios PT, editor. *Extractive and Azeotropic Distillation. Advances in Chemistry*, Washington, DC: American Chemical Society, 1974:35–45.
21. Ligero EL, Ravagnani TMK. Simulation of salt extractive distillation with spray dryer salt recovery for anhydrous ethanol production. *J Chem Eng Jpn*. 2002;35:557–563.
22. Hussain MAM, Anthony JL, Pfromm PH. Reducing the energy demand of corn-based fuel ethanol through salt extractive distillation enabled by electrodialysis. *AIChE J*. 2012;58:163–172.
23. Kolat RS, Hudson RK. Method of producing substantially dust free calcium chloride particulate. U.S. Patent 3,732,082(A), 1973.
24. Smeets B, Iype E, Nedea SV, Zondag HA, Rindt CCM. A DFT based equilibrium study on the hydrolysis and the dehydration reactions of $MgCl_2$ hydrates. *J Chem Phys*. 2013;139:124312.
25. Sugimoto K, Dinnebier RE, Hanson JC. Structures of three dehydration products of bischofite from in situ synchrotron powder diffraction data ($MgCl_2 \cdot nH_2O$; n=1, 2, 4). *Acta Crystallogr B Struct Sc*. 2007;63:235–242.
26. Rieder RM, Thompson AR. Salt effect in vapor-liquid equilibria. ethanol-water saturated with potassium nitrate. *Ind Eng Chem*. 1950; 42:379–382.
27. Vercher E, Peña MP, Martinez-Andreu A. Isobaric vapor-liquid equilibrium for ethanol + water + potassium nitrate. *J Chem Eng Data*. 1996;41:66–69.
28. Vercher E, Muñoz R, Martinez-Andreu A. Isobaric vapor-liquid equilibrium data for the ethanol-water-potassium acetate and ethanol-water-(potassium acetate/sodium acetate) systems. *J Chem Eng Data*. 1991;36:274–277.
29. Meyer T, Polka HM, Gmehling J. Low-pressure isobaric vapor-liquid equilibria of ethanol/water mixtures containing electrolytes. *J Chem Eng Data*. 1991;36:340–342.
30. Balaban A, Kuranov G, Smirnova N. Phase equilibria modeling in aqueous systems containing 2-propanol and calcium chloride or/and magnesium chloride. *Fluid Phase Equilib*. 2002;194–197:717–728.
31. Chen CC, Mathias PM, Orbey H. Use of hydration and dissociation chemistries with the electrolyte–NRTL model. *AIChE J*. 1999;45: 1576–1586.
32. Robinson RA, Stokes RH. *Electrolyte Solutions*, 2nd ed. London: Butterworths Scientific Publications, 1959.
33. Stokes RH, Robinson RA. Ionic hydration and activity in electrolyte solutions. *J Am Chem Soc*. 1948;70:1870–1878.
34. Conway BE. *Ionic Hydration in Chemistry and Biophysics*. Amsterdam: Elsevier Scientific Publishing, 1981.
35. Jansz JJC. Estimation of ionic activities in chloride systems at ambient and elevated temperatures. *Hydrometallurgy*. 1983;11:13–31.
36. Lu XH, Maurer G. Model for describing activity coefficients in mixed electrolyte aqueous solutions. *AIChE J*. 1993;39:1527–1538.
37. Lu XH, Zhang LZ, Wang YR, Shi J, Maurer G. Prediction of activity coefficients of electrolytes in aqueous solutions at high temperatures. *Ind Eng Chem Res*. 1996;35:1777–1784.
38. Zhao J, Dong CC, Li CX, Meng H, Wang ZH. Isobaric vapor-liquid equilibria for ethanol-water system containing different ionic liquids at atmospheric pressure. *Fluid Phase Equilib*. 2006;242: 147–153.
39. Li GZ, Hu YF, Liu YS, Li GL, Tang YX, Wu LH, Shi CF, Xu K. Isobaric vapor–liquid equilibrium for the ternary system (formaldehyde + 1,3-dioxolane + water) at 101.3 kPa. *J Chem Eng Data*. 2013;58:2854–2860.
40. Li G, Li ZB. Measurement and modeling of vapor–liquid equilibria for the octane + sulfuric acid + water + ethanol system. *J Chem Eng Data*. 2013;58:2044–2050.
41. Li G, Li ZB, Asselin E. Determination and modeling of vapor–liquid equilibria for the sulfuric acid + water + butyl acetate + ethanol system. *Ind Eng Chem Res*. 2013;52:3481–3489.
42. Li G, Li ZB. Determination and prediction of vapor–liquid equilibria for a system containing water + butyl acetate + cyclohexane + ethanol. *J Chem Eng Data*. 2012;57:2543–2548.
43. Sun HY, Fang WJ, Guo YS, Lin RS. Investigation of bubble-point vapor pressures for mixtures of an endothermic hydrocarbon fuel with ethanol. *Fuel*. 2005;84:825–831.
44. Gao WC, Li ZB. A practical approach to produce Mg-Al spinel based on the modeling of phase equilibria for NH_4Cl-$MgCl_2$-$AlCl_3$-H_2O system. *AIChE J*. 2013;59:1855–1867.
45. Smirnova NA. Phase equilibria modeling in aqueous-organic electrolyte systems with regard to chemical phenomena. *J Chem Thermodyn*. 2003;35:747–762.
46. Ohe S. Prediction of salt effect on vapor–liquid equilibria. *Fluid Phase Equilib*. 1998;144:119–129.
47. Takamatsu H, Ohe S. Modified solvation model for salt effect on vapor–liquid equilibria. *Fluid Phase Equilib*. 2002;194–197:701–715.
48. Pinsky ML, Gruber G. Phase equilibria in aqueous systems containing Na^+, K^+, Mg^{+2}, Cl^-, and SO_4^{-2} ions using the NRTL model. *AIChE Symp. Ser. 298,* 1994;90:112–126.
49. Hunt JP, Friedman HL. Aquo complexes of metal ions. In: Lippard SJ, editor. *Progress in Inorganic Chemistry*. Chichester: John Wiley, 1983:359–387.
50. Enderby JE, Cummings S, Herdman GJ, Neilson GW, Salmon PS, Skipper N. Diffraction and the study of aqua ions. *J Phys Chem*. 1987;91:5851–5858.
51. Soave G. Equilibrium constants from a modified Redlich-Kwong equation of state. *Chem Eng Sci*. 1972;27:1197–1203.
52. Wang PM, Anderko A, Young RD. A speciation-based model for mixed-solvent electrolyte systems. *Fluid Phase Equilib*. 2002;203: 141–176.
53. Tanger JC, Helgeson HC. Calculation of the thermodynamic and transport properties of aqueous species at high pressures and temperatures; revised equations of state for the standard partial molal properties of ions and electrolytes. *Am J Sci*. 1988;288: 19–98.
54. Wang P, Kosinski JJ, Anderko A, Springer RD, Lencka MM, Liu J. Ethylene glycol and its mixtures with water and electrolytes: thermodynamic and transport properties. *Ind Eng Chem Res*. 2013;52: 15968–15987.
55. Carey JS, Lewis WK. Studies in distillation. *Ind Eng Chem*. 1932; 24:882–883.
56. Kurihara K, Nakamichi M, Kojima K. Isobaric vapor-liquid equilibria for methanol + ethanol + water and the three constituent binary systems. *J Chem Eng Data*. 1993;38:446–449.
57. Mohs A, Gmehling J. A revised LIQUAC and LIFAC model (LIQUAC*/LIFAC*) for the prediction of properties of electrolyte containing solutions. *Fluid Phase Equilib*. 2013;337:311–322.
58. Sako T, Hakuta T, Yoshitome H. Vapor pressures of binary (water-hydrogen chloride, -magnesium chloride, and -calcium chloride) and ternary (water-magnesium chloride-calcium chloride) aqueous solutions. *J Chem Eng Data*. 1985;30:224–228.
59. Rard JA, Miller DG. Isopiestic determination of the osmotic and activity coefficients of aqueous magnesium chloride solutions at 25°C. *J Chem Eng Data*. 1981;26:38–43.

Manuscript received May 9, 2014, and revision received Oct. 8, 2014.